

# *Ab-initio* calculation of effective exchange interactions, spin waves, and Curie temperature in L<sub>21</sub>- and L<sub>12</sub>-type local moment ferromagnets

I. Galanakis · E. Şaşıoğlu

Received: date / Accepted: date

**Abstract** Employing first-principles electronic structure calculations in conjunction with the frozen-magnon method we study the effective exchange interactions and spin waves in local moment ferromagnets. As prototypes we have chosen three L<sub>21</sub>-type full Heusler alloys Cu<sub>2</sub>MnAl, Ni<sub>2</sub>MnSn and Pd<sub>2</sub>MnSn, and the L<sub>12</sub>-type XPt<sub>3</sub> compounds with X= V, Cr and Mn. We have also included CoPt<sub>3</sub> which is a usual ferromagnet. In all compounds due to the large spatial separation ( $\sim 4 \text{ \AA}$ ) of the magnetic transition metal atoms, the *3d* states belonging to different atoms overlap weakly and as a consequence the exchange coupling is indirect, mediated by the *sp* electrons. Calculated effective exchange parameters are long range and show RKKY-type oscillations. The spin-wave dispersion curves are in reasonable agreement with available experimental data. Using the calculated exchange parameters we have estimated the Curie temperatures within both the mean-field and the random-phase approximations. In local moment ferromagnets deviations of the estimated Curie temperature with respect to the available experimental data occur when the ground-state electronic structure calculations overestimate the values of the spin magnetic moments as in VPt<sub>3</sub>.

**Keywords** Exchange interactions · Spin waves · Magnons · Local moment ferromagnets · Curie temperature

## 1 Introduction

*Ab-initio* (first-principles) electronic structure calculations based on the density functional theory (DFT) have been widely employed during the last decades to analyze the behavior of a constantly increasing number of alloys. The rapid development of computer resources available to scientists allowed to study systems with increasing complexity. In the meantime electronic structure calculations have served to predict new materials with novel properties susceptible of finding applications in modern nanotechnology which, very often, were grown using modern experimental techniques like Molecular Beam Epitaxy or Pulsed Layered Deposition. First-principles calculations cover a wide range of materials from metals and semiconductors to biological systems. Also magnetic materials have been widely studied using such methods and their properties connected to the spin of the electrons, *e.g.* spin moments, magnetic anisotropy energy, magneto-optical properties, etc, have been accurately represented.

The drawback of first-principles electronic structures calculations stems from density functional theory which has been developed for zero temperature. For realistic applications temperature plays a crucial role since it greatly affects magnetic properties, *e.g.* the magnetization of a material drops with temperature and vanishes at the Curie temperature. Thus it becomes more and more important to use the results of *ab-initio* calculations as the basis for developing complex methodologies to study the temperature effect on the electronic prop-

---

I. Galanakis  
Department of Materials Science, School of Natural Sciences,  
University of Patras, GR-26504 Patra, Greece  
E-mail: galanakis@upatras.gr

E. Şaşıoğlu  
Peter Grünberg Institut and Institute for Advanced Simulation,  
Forschungszentrum Jülich and JARA, 52425 Jülich,  
Germany and Department of Physics, Fatih University,  
34500, Büyükçekmece, İstanbul, Turkey  
E-mail: e.sasioglu@fz-juelich.de

erties of materials. To study thermodynamics properties of magnetic materials the obtained zero temperature electronic structure results is usually mapped onto classical Heisenberg Hamiltonian, which can be solved by employing the methods of statistical physics [1, 2, 3, 4, 5, 6, 7, 8, 9, 10].

So far two methods have been widely used to calculate effective exchange interactions in magnetic materials within the adiabatic approximation: (i) the frozen-magnon approach, which is a reciprocal space method [11] and (ii) the Lichtenstein's real space method [12]. The common ground of both approaches is that only the collective excitations, known as magnons, are taken into account. These excitations dominate the lower part of the excitation spectra and correspond to spin-waves which run through the materials and which are associated to the orientation of the spin moments. Except magnons, in magnetic materials exist the so-called Stoner excitations which are associated to excitations of single majority-spin electrons to unoccupied minority-spin states and thus are accompanied by the flip of the electrons spin [13]. In most systems based on transition-metal atoms the contribution of the Stoner excitations to the lower part of the excitation is weak due to the large exchange splitting of these atoms and in some cases like the half-metallic ferromagnets they are even separated by a large Stoner gap from magnons [14]; as Stoner gap is defined the energy difference between the highest occupied majority-spin state and the lowest unoccupied minority-spin state and thus corresponds to the lowest possible Stoner excitation energy.

## 2 Method and motivation

As we mentioned above the lower part of the excitation spectra is dominated by the so-called magnons which involve collective excitations of the spin magnetic moments. In a simplified picture we can assume that the magnitude of the spin magnetic moments of the atoms does not change with respect to the zero Kelvin value calculated using ab-initio electronic structure methods but as we raise temperature atomic spin moments change their orientation in such a way that the azimuthal angle can be described by a propagating plane wave characterized by a vector  $\mathbf{q}$  belonging in the Brillouin zone. This is the so-called spin-wave or magnon. If the magnitude of  $\mathbf{q}$  is small we can assume that the energy for the creation of the spin-wave is given by the relation  $E(\mathbf{q}) = D|\mathbf{q}|^2$  and thus depends only on the magnitude of the wave vector and not its orientation in the Brillouin zone; this usually occurs around the  $\Gamma$  point as we will show also later on when presenting the energy-dispersion of the spin waves. The constant  $D$  is

referred to as the "spin-wave stiffness constant". Typical values of  $D$  for transition metals are about 300-600 meV  $\text{\AA}^2$  [15].

The ground-state electronic structure calculations are carried out using the augmented spherical waves method (ASW) [16] within the atomic-sphere approximation (ASA) [17] and the exchange-correlation potential is chosen in the generalized gradient approximation [18]. The method of the calculation of the exchange constants within the frozen-magnon approximation has been already presented elsewhere [19]. Here, to make the paper reasonably self-contained a brief overview is given. Notice that since the magnetism is almost exclusively concentrated on the transition metal site in the compounds under study (with the exception of  $\text{CoPt}_3$ ), as confirmed also from our calculations presented in the next sections, the equations presented below are for systems with only one magnetic sublattice for reasons of simplicity.

To calculate the interatomic exchange interactions we use the frozen-magnon technique [11] and map the results of the calculation of the total energy of the helical magnetic configurations

$$\mathbf{s}_n = (\cos(\mathbf{q}\mathbf{R}_n) \sin \theta, \sin(\mathbf{q}\mathbf{R}_n) \sin \theta, \cos \theta) \quad (1)$$

onto a classical Heisenberg Hamiltonian

$$H_{eff} = - \sum_{i \neq j} J_{ij} \mathbf{s}_i \cdot \mathbf{s}_j \quad (2)$$

where  $J_{ij}$  is an exchange interaction between two Mn(X) atoms and  $\mathbf{s}_i$  is the unit vector pointing in the direction of the magnetic moment at site  $i$ ,  $\mathbf{R}_n$  are the lattice vectors,  $\mathbf{q}$  is the wave vector of the helix and  $\theta$  the polar angle giving the deviation of the moments from the  $z$  axis. Within the Heisenberg model (2) the energy of the frozen-magnon configurations can be represented in the form

$$E(\theta, \mathbf{q}) = E_0(\theta) - \sin^2 \theta J(\mathbf{q}) \quad (3)$$

where  $E_0$  does not depend on  $\mathbf{q}$  and  $J(\mathbf{q})$  is the Fourier transform of the parameters of exchange interaction between pairs of magnetic atoms:

$$J(\mathbf{q}) = \sum_{\mathbf{R} \neq 0} J_{0\mathbf{R}} \exp(i\mathbf{q} \cdot \mathbf{R}). \quad (4)$$

Calculating  $E(\theta, \mathbf{q})$  for a regular  $\mathbf{q}$ -mesh in the Brillouin zone of the crystal and performing back Fourier transformation one gets exchange parameters  $J_{0\mathbf{R}}$  between pairs of the magnetic atoms.

First, the Curie temperature is estimated within the mean-field approximation (MFA). For the case of a material with one magnetic sublattice (for the multi-sublattice case see Refs. [19, 21]) the equation is

$$k_B T_C^{\text{MFA}} = \frac{2}{3} \sum_{\mathbf{R} \neq 0} J_{0\mathbf{R}}. \quad (5)$$

Within the random phase approximation (RPA) the Curie temperature is given by the relation [15]

$$\frac{1}{k_B T_C^{\text{RPA}}} = \frac{6\mu_B}{M} \frac{1}{N} \sum_{\mathbf{q}} \frac{1}{\omega(\mathbf{q})}, \quad (6)$$

where  $\omega(\mathbf{q}) = 4/M[J(0) - J(\mathbf{q})]$  is the energy of spin-wave excitations,  $\mu_B$  is the Bohr magneton,  $N$  is the number of  $\mathbf{q}$  points in the first Brillouin zone, and  $M$  is the atomic magnetic moment. Within the RPA formalism as implemented in our method it is not possible to take into account multiple magnetic sublattices contrary to the implementation of MFA. Finally we should note that MFA corresponds to an equal weighting of the low- and high-energy spin-wave excitations leading to an overestimation of the experimental Curie temperature contrary to RPA where the lower-energy excitations make a larger contribution to the Curie temperature leading to more realistic values [15, 22, 23].

We have applied the frozen-magnon approximation to a variety of systems. The obtained Curie temperatures were found to be in good agreement with available experimental data when the Stoner gap was large enough so that magnons are well-separated from Stoner excitations in the excitation spectra. Such systems are the half-metallic ferro-, ferri- and antiferromagnetic compounds where the majority-spin band is metallic and the minority-spin band is semiconducting. The gap at the Fermi level in minority-spin band leads to a large value of the Stoner gap. Half-metallic systems where we have applied our method include the diluted magnetic semiconductors [11], ferromagnetic Heusler alloys like NiMnSb and Co<sub>2</sub>MnSi [22, 23, 24, 25], half-metallic antiferromagnets [26, 27], transition metal pnictides and chalcogenides [25, 28, 29, 30], and half-metallic sp-electron ferromagnets [14, 31, 32]. Moreover these results have served to study several other thermodynamics properties like the temperature dependence of the magnetization in half-metallic antiferromagnets [33] or the thermal properties of the Ni sublattice in NiMnSb [34]. Local ferromagnets which have been studied include the Mn-based semi and full Heusler alloys like NiMnSb and Ni<sub>2</sub>MnGa [19, 35, 36]. As shown in Ref. [37] the Mn  $d$  states are strongly delocalized and hybridize with the  $d$  and  $p$  electrons of the neighboring transition-metal and sp atoms, respectively. The localization of the spin magnetic moment comes from the fact that minority-spin electrons are almost excluded from the Mn site while almost all majority-spin states are occupied.

In this article we consider two classes of local-moment ferromagnets: (i) the full-Heusler alloys Cu<sub>2</sub>MnAl, Ni<sub>2</sub>MnSnPd<sub>2</sub>MnSn studied by Noda and Ishikawa in 1976 [55]. and Pd<sub>2</sub>MnSn crystallizing in the L<sub>21</sub> structure, and (ii) the XPt<sub>3</sub> alloys in the L<sub>12</sub> structure with X= V, Cr, Mn and Co. Both lattice structures are cubic and have the

same symmetry group as the fcc lattice. The Mn-based compounds have attracted a lot of interest due to the localized nature of Mn spin moments [37]. The XPt<sub>3</sub> compounds on the other hand have also attracted considerable attention both theoretically [38, 39, 40, 41, 42, 43, 44, 45] and experimentally [46, 47, 48, 49, 50, 51, 52, 53] due to the variety of magnetic order which they exhibit and due to the large magnetocrystalline anisotropy shown by CrPt<sub>3</sub> [44] and CoPt<sub>3</sub> [50] which makes the latter alloys attractive for magnetic storage devices. Moreover these systems are prototypes for studying the induced magnetism at the Pt site due to the strong hybridization between the  $d$ -orbitals of the transition-metal atoms and the platinum atoms [40]. Note that when X=V, Cr, Mn or Co the compounds are ferromagnets (the compounds with V, Cr and Mn are also local moment ferromagnets) [46, 47, 49], while the FePt<sub>3</sub> shows antiferromagnetism [48] and this is why we have not included it in our study.

Due to the variety of compounds under investigation and to help the reader we present in the next section first the results for the three Heusler compounds and MnPt<sub>3</sub> for which the magnetism is concentrated at the Mn site and in Section 4 we compare the obtained results for MnPt<sub>3</sub> with the rest of the XPt<sub>3</sub> alloys.

### 3 Mn-based alloys

Alloys where coexist Mn atoms with sp atoms and/or late transition metal atoms are susceptible of being local ferromagnets; the majority-spin electronic band of Mn atoms is almost completely filled while the charge at the minority-spin band is negligible and as a result minority-spin electrons are excluded from the Mn site leading to a localization of the Mn spin moment. Local spin magnetic moments do not necessarily mean that Mn  $d$ -electrons are localized and as shown by Kübler *et al.* in Ref. [37] the Mn  $d$ -orbitals are strongly delocalized due to their strong hybridization with the neighboring  $d$  and  $p$  orbitals. Prototypes for local ferromagnetism are the full Heusler alloys like Cu<sub>2</sub>MnAl or Ni<sub>2</sub>MnAl which have been extensively studied in [37]. Here we will focus on compounds for which the experimental dispersion curve of the magnons for crystals is known and thus can be compared to our calculated results. We have chosen three Heusler alloys crystallizing in the L<sub>21</sub> structure which consists of four interpenetrating fcc sublattices: Cu<sub>2</sub>MnAl which has been experimentally studied by Tajima *et al.* in 1977 [54], and Ni<sub>2</sub>MnSn and Pd<sub>2</sub>MnSn studied by Noda and Ishikawa in 1976 [55]. We have also included in our study the cubic MnPt<sub>3</sub> alloy studied by Paul and Stirling in 1979 [56] which crystallizes in the so-called L<sub>12</sub> structure. For the three

**Table 1** Lattice parameter  $a$  (in Å) used in the calculations, atom-resolved and total spin magnetic moments (in  $\mu_B$ ), and both calculated and experimental Curie temperatures (in K) for the local moment ferromagnets under study and  $\text{CoPt}_3$  which is a usual ferromagnet. Note that for the calculation of the Curie temperature we have employed both the mean-field (MFA) and random-phase (RPA) approximations and we have considered only Mn-Mn or X-X interactions except the cases of  $\text{MnPt}_3$  and  $\text{CoPt}_3$  for which we present in parenthesis also the values with the MFA taking into account also the Mn(Co)-Pt and Pt-Pt interactions. Lattice constants and experimental data come from Refs [46], [47], [49], [54], [55] and [56].

Compound	$a$	$m_{(\text{Cu,Ni,Pd})}$	$m_{\text{Mn}}$	$m_{(\text{Al,Sn})}$	$m_{\text{Total}}$	$T_C^{\text{MFA}}$	$T_C^{\text{RPA}}$	$T_C^{\text{Exp}}$
$\text{Cu}_2\text{MnAl}$	5.95	0.02	3.67	-0.11	3.60	970	635	603
$\text{Ni}_2\text{MnSn}$	6.05	0.21	3.73	-0.06	4.09	320	254	360
$\text{Pd}_2\text{MnSn}$	6.38	0.07	4.08	-0.06	4.16	252	178	189
Compound	$a$	$m_{\text{X}}$	$m_{\text{Pt}}$	$m_{\text{Total}}$	$T_C^{\text{MFA}}$	$T_C^{\text{RPA}}$	$T_C^{\text{Exp}}$	
$\text{VPt}_3$	3.870	1.564	-0.089	1.296	740	631	290	
$\text{CrPt}_3$	3.877	2.871	-0.071	2.658	834	662	494	
$\text{MnPt}_3$	3.898	3.863	0.131	4.257	406(414)	317	390	
$\text{CoPt}_3$	3.854	1.776	0.268	2.580	145(220)	130	288	

Heusler compounds we have used the experimental lattice constants and for  $\text{MnPt}_3$  the lattice constant given in Ref. [38] (see Table 1 for the values). For all calculations we have used a dense  $30 \times 30 \times 30$  grid in the Brillouin zone to carry out the needed integrations in the reciprocal space.

For all four compounds the spin magnetic moment is localized at the Mn site as shown in Table 1 and the other sites carry a negligible spin moment with respect to the Mn atoms. The Mn spin moment varies from 3.67 to 4.08  $\mu_B$  and the small variation is due to the effect of the local environment (the degree of hybridization with the orbitals of the neighboring atoms). We do not present for the Heusler alloys the atom-resolved and total density of states (DOS) since it is similar to the ones in Ref. [37]. Relevant to our discussion is the Mn-resolved DOS, which varies little between the four compounds under study and in Fig. 3 we present the total and Mn-resolved DOS in  $\text{MnPt}_3$ . The Mn majority-spin states are almost completely occupied while the minority states are completely empty; there is a very small weight of minority-spin occupied states due to the influence of the neighboring Pt atoms but this does not change the overall picture.

Although a real Stoner gap does not exist as in half-metals, due to the  $sp-d$  mixing the majority-spin DOS below the Fermi level in the  $\text{L2}_1$ -type compounds (see Ref. [36]) and the minority-spin DOS just above the Fermi level in the  $\text{L1}_2$ -type compounds (see Fig. 3) are almost negligible; an exception occurs as shown in Fig. 3 for  $\text{CoPt}_3$  which is not a local moment ferromagnet and substantial part of the Co minority-spin states are occupied. Therefore, the single-particle spin-flip Stoner excitations for the local ferromagnets make a small contribution to the total excitation spectra at low energies, where collective spin-wave modes dominates. As

**Table 2** Calculated ( $D_{\text{th}}$ ) and experimental ( $D_{\text{th}}$ ) spin-wave stiffness constant for four local ferromagnets. Experimental data come from Refs [54], [55] and [56].

Compound	Structure	$D_{\text{th}}(\text{meV}\text{\AA}^2)$	$D_{\text{ex}}(\text{meV}\text{\AA}^2)$
$\text{Cu}_2\text{MnAl}$	$\text{L2}_1$	240	167
$\text{Ni}_2\text{MnSn}$	$\text{L2}_1$	166	154
$\text{Pd}_2\text{MnSn}$	$\text{L2}_1$	138	123
$\text{MnPt}_3$	$\text{L1}_2$	260	270

a result, well defined spin waves exist throughout the Brillouin zone with small damping as observed in experiments (see Fig.1), which also justifies the use of the frozen-magnon method in the calculation of the spin-wave dispersion and the exchange interactions. Indeed, recent time-dependent DFT calculation of spin-wave dispersion of  $\text{Cu}_2\text{MnAl}$  gave very similar results to the one obtained from the adiabatic approximation, *i.e.*, Liechtenstein formula [20].

In Fig. 1 we present the calculated spin-waves dispersion energy  $\omega(\mathbf{q})$  curves and we compare them with the available experimental data from Refs [54,55,56] employing the neutrons diffraction technique. Note that experiments have been carried out for different temperature from 4.2 K for  $\text{Cu}_2\text{MnAl}$  up to 80 K for  $\text{MnPt}_3$ . A close look at the results in Ref. [55] reveals that as the temperature rises for the same  $\mathbf{q}$  experiments give a smaller  $\omega(\mathbf{q})$  value. Overall the calculated dispersion curves follow the behavior of the experimental data with the minimum at the  $\Gamma$  point. For the three Heusler alloys our calculations give larger values of the dispersion energies  $\omega(\mathbf{q})$ , except close to the  $\Gamma$  point where calculations accurately represent the experimental data. For  $\text{MnPt}_3$  calculated and experimental data fall one on top of the other except close to the R point, but this agreement is misleading since the experiment

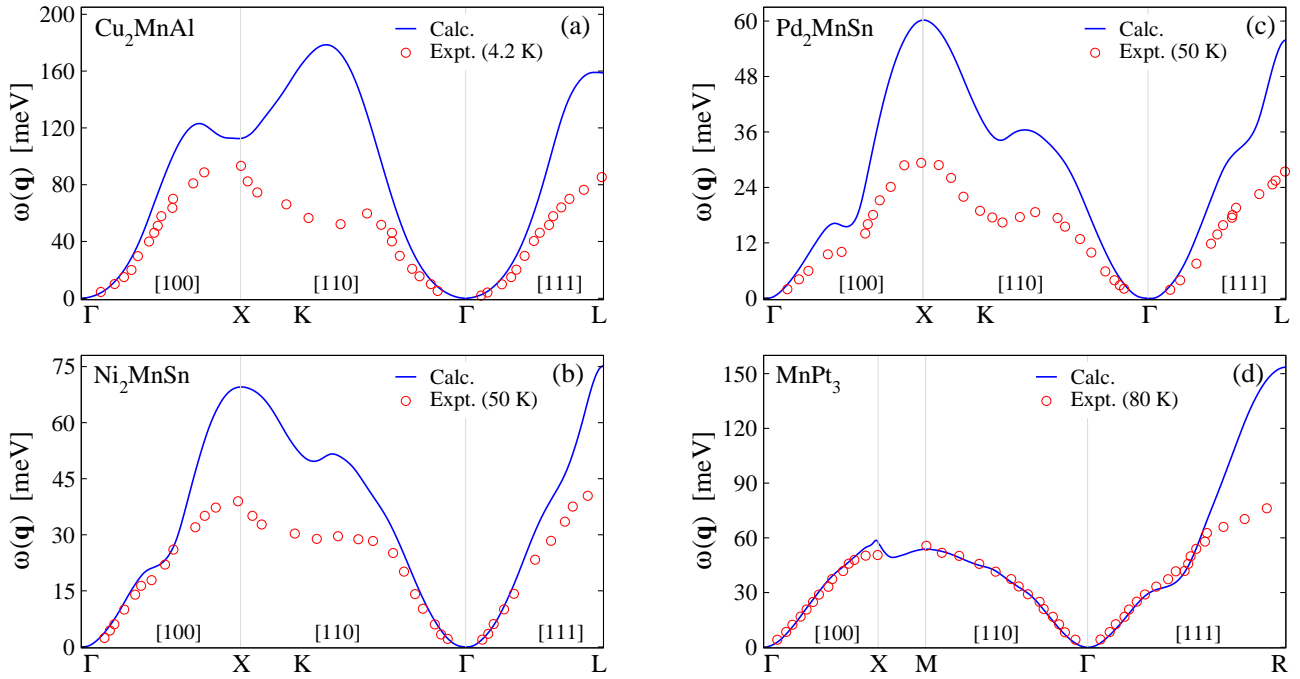


**Fig. 1** Calculated (solid lines) spin-wave dispersion curves in the first Brillouin zone along high-symmetry axis for the local-moment ferromagnets. The experimental data (open circles) have been reproduced from Ref. [54] for Cu<sub>2</sub>MnAl, Ref. [55] for Ni<sub>2</sub>MnSn and Pd<sub>2</sub>MnSn and Ref. [56] for MnPt<sub>3</sub>. Note that experimental data have been measured at different temperatures.

has been carried out at 80 K much higher than for Cu<sub>2</sub>MnAl. The good representation of the experimental data by the calculations can be traced at the spin-wave stiffness constants  $D$  which are presented in Table 2. As we mentioned above the  $D$  is the constant connecting the energy needed for the creation of the spin-wave when the magnitude of the wave-vector  $\mathbf{q}$  is small as it occurs around the  $\Gamma$  point. We get the largest discrepancy for Cu<sub>2</sub>MnAl where theory and experiment give values of 240 and 167 meV  $\text{\AA}^2$ , respectively, while for the other three compounds theory overestimates the value of  $D$  by less than 15 meV  $\text{\AA}^2$ .

From the spin-waves dispersion energies we can calculate the exchange constants describing the effective Mn-Mn exchange interactions as discussed in the previous section. In Fig. 2 we present their values as a function of the distance between the Mn atoms. In all compounds due to the large spatial separation ( $\sim 4 \text{\AA}$ ) of the magnetic transition metal atoms the  $3d$  states belonging to different atoms overlap weakly and as a consequence the exchange coupling is indirect, mediated by the  $sp$  electrons. A very nice discussion on the exchange coupling in local moment ferromagnets can be found in Ref. [36]. As seen from Fig. 2 the calculated effective exchange parameters are long range and show RKKY-type oscillations. All compounds show tendency to ferromagnetism but the different behavior of the exchange constants as a function of the dis-

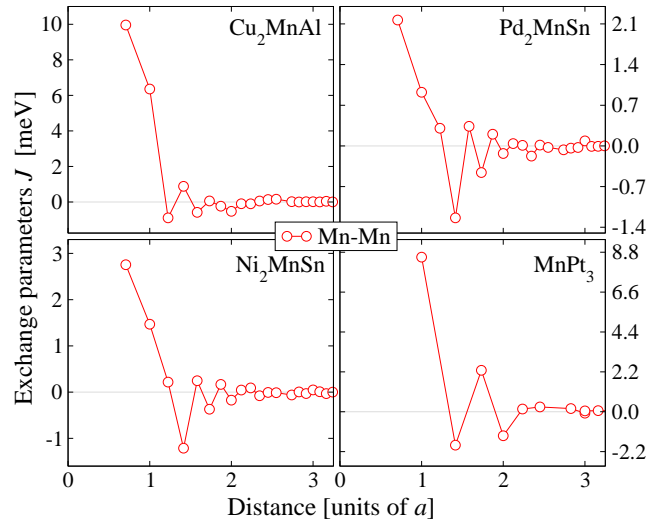


**Fig. 2** Mn-Mn exchange constants in the four Mn-based local-moment ferromagnets under study as a function of their distance. The distance is given in units of the lattice parameter:  $a$ .

tance strongly influences the Curie temperatures and thus the temperature behavior of the magnetization. In Table 1 we have also gathered the Curie temperature within both the MFA and RPA approaches together with the experimental values from Refs [54,55,56]. In MFA all magnons contribute equally to the Curie temperature, while in RPA the magnons with the lower energy have a higher contribution as can be deduced

by the equations in the previous section. Thus RPA is expected to give a more accurate description of the Curie temperature. For  $\text{Cu}_2\text{MnAl}$ , as shown in Fig. 2, the coupling between Mn nearest and next-nearest neighbors is strongly ferromagnetic reaching a value of 10 meV for nearest neighboring Mn atoms and it almost vanishes for more distant Mn atoms. Thus the ferromagnetism in  $\text{Cu}_2\text{MnAl}$  is extremely stable and the RPA calculated Curie temperature is 635 K well above the room temperature and close to the experimental value of 603 K. The Curie temperature calculated within MFA is more than 50% larger than the RPA value. In both  $\text{Pd}_2\text{MnSn}$  and  $\text{Ni}_2\text{MnSn}$  the interactions between a Mn atom and up to its third neighbors are positive while between the Mn atoms fourth neighbors it is negative; for further distance it is much smaller. Note also that the scale in the vertical axis is different than  $\text{Cu}_2\text{MnAl}$  and the maximum value is about 2-3 meV. Since the number of fourth neighbors is large with respect to the closest neighbors, ferromagnetism in these two Heusler compounds is not as robust as in  $\text{Cu}_2\text{MnAl}$  and the Curie temperature is close to the room temperature for  $\text{Ni}_2\text{MnSn}$  and below room temperature for  $\text{Pd}_2\text{MnSn}$  for which the antiferromagnetic interaction between Mn atoms fourth neighbors is larger in magnitude.  $\text{MnPt}_3$  exhibits strong ferromagnetic coupling between Mn atoms nearest neighbors while for Mn second and third neighbors the coupling is same in magnitude but of opposite sign. Thus the nearest neighbors interaction stabilizes ferromagnetic order with an experimental Curie temperature around 390 K. Note that for  $\text{Ni}_2\text{MnSn}$ ,  $\text{Pd}_2\text{MnSn}$  and  $\text{MnPt}_3$  where the tendency to ferromagnetism is not as strong as for  $\text{Cu}_2\text{MnAl}$  MFA gives values for the Curie temperature closer to the experimental ones than PRA although the latter one is in-principle more exact. This behavior is contrary to the behavior of the compounds regarding the spin-wave stiffness constants, since for the latter only the region around the  $\Gamma$  point is important while for the calculation of the Curie temperature we take into account the dispersion of the spin-wave energy in the whole Brillouin zone.

#### 4 $\text{XPt}_3$ alloys

In Fig. 3 we present the X-resolved and total DOS for all compounds under study and in Fig. 4 the calculated exchange constants. In the lower part of Table 1 we have gathered the lattice constants used for the calculations, the atom-resolved and total spin magnetic moments, the Curie temperature within both MFA and RPA as well as the experimental Curie temperature. We will start our discussion from the DOS of the local

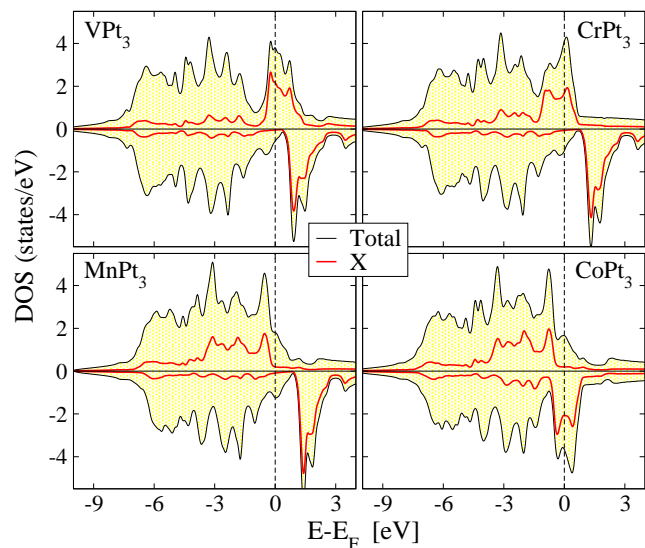


**Fig. 3** Total and transition-metal resolved DOS for the six cubic  $\text{XPt}_3$  ferromagnets under study. Positive DOS values are assigned to the majority spin electrons and negative DOS values to the minority spin electrons.

moment ferromagnets ( $X = \text{V}, \text{Cr}$  and  $\text{Mn}$ ) presented in Fig. 3. As we move from V to Cr and then to Mn the extra electrons occupy majority-spin states and the minority-spin states are above the Fermi level. This is also reflected on the X-resolved spin magnetic moments in Table 1 where from V to Cr the transition-metal spin magnetic moment increases by  $\sim 1.3 \mu_B$  and from Cr to Mn by about  $1 \mu_B$ . Since the majority-spin states in  $\text{VPt}_3$  and  $\text{CrPt}_3$  are not completely occupied these alloys should be classified as weak ferromagnets contrary to  $\text{MnPt}_3$  where all Mn majority-spin states are occupied. In all three alloys the Pt atoms have induced spin magnetic moments two orders of magnitude smaller than the X atoms and thus are not relevant for the discussion of the Curie temperature. To make this point clear we have calculated for  $\text{MnPt}_3$  the Curie temperature within MFA taking into account only the Mn-Mn interactions and all Mn-Mn, Mn-Pt and Pt-Pt interactions and the value changed from 406 K to 414 K and thus Mn-Mn interactions are the dominant ones and the Pt sublattice can be neglected in the latter discussion. The MFA values for both  $\text{VPt}_3$  and  $\text{CrPt}_3$  are much larger than the RPA ones by more than 100 K as expected from the discussion in Section 2. But as we move from Mn to Cr and then to V the discrepancy between the RPA values and the experimental ones increases. The difference should be traced in the experimental spin magnetic moments associated to these Curie temperatures. In Ref. [49]  $\text{VPt}_3$  shows a Curie temperature of 290 K and Vanadium atoms a spin magnetic moment of about  $1.0 \mu_B$ ; both values

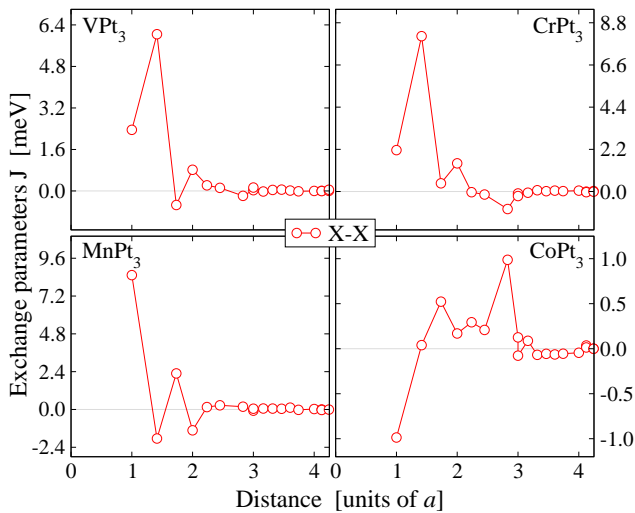


**Fig. 4** X-X exchange constants for the XPt<sub>3</sub> alloys under study as a function of their distance. Details as in Fig. 2.

are much smaller than our calculated values of 631 K and  $1.56 \mu_B$ . For CrPt<sub>3</sub>(MnPt<sub>3</sub>) the experimental values in Ref. [46] are 494(390) K and  $2.33(3.60) \mu_B$ . Thus as we move from V to Mn the calculated spin magnetic moments come closer to the experimental values and so do the Curie temperatures. The large discrepancy exhibited for V is a well-known problem of density-functional-theory-based calculations and can be traced also to other V-based compounds [45]. Regarding the exchange parameters in Fig. 4 V-V and Cr-Cr interactions present a similar picture with nearest and next-nearest neighbors being ferromagnetically coupled and the coupling is stronger for second than first neighboring transition metal atoms. For MnPt<sub>3</sub> as we discussed in Section 3 nearest neighbors present a strong ferromagnetic coupling while Mn-Mn next-nearest neighbors are antiferromagnetically coupled.

In CoPt<sub>3</sub>, like MnPt<sub>3</sub>, all transition-metal majority-spin states are occupied but contrary to the latter alloy significant part of the Co minority-spin states is also occupied and CoPt<sub>3</sub> cannot be classified as a local moment ferromagnet. The exchange splitting between the Co majority- and minority-spin electronic bands is smaller than for Mn in MnPt<sub>3</sub> due to the extra electrons which fill also minority-spin states. Moreover Pt atoms carry now a significant induced spin magnetic moment of about  $0.27 \mu_B$  about one sixth of the Co spin magnetic moment and thus both Co-Pt and Pt-Pt interactions are now important to calculate the temperature dependent properties. The Co-Co exchange constants presented in Fig. 4 show a peculiar behavior since they are negative for nearest-neighbors, vanishing for next-nearest neighbors and positive for further neighbors. This behavior stems from the strong interplay be-

tween the ferromagnetic RKKY and antiferromagnetic superexchange interactions [35, 36] and although finally CoPt<sub>3</sub> is ferromagnetic the Curie temperature is smaller than the room temperature. Experiments in Ref. [47] give a value of 288 K while our RPA and MFA values taking into account only the Co-Co interactions are 130 K and 145 K respectively. However, the multi-sublattice MFA gives a value of 220 K considerably larger than the 145 K calculated taking into account only the Co-Co interactions. The multisublattice RPA is expected to give a  $T_c$  below 200 K. The discrepancy for CoPt<sub>3</sub> should be attributed to the underestimation of the exchange interactions in the frozen-magnon method in the case of small magnetic moments [57]. It is more likely that the Co-Pt exchange interactions are underestimated due to the small Pt magnetic moments.

## 5 Conclusions

Combining first-principles electronic structure calculations and the frozen-magnon approximation we have studied the thermodynamic properties of two classes of local moment ferromagnets (i) the Heusler alloys Cu<sub>2</sub>MnAl, Ni<sub>2</sub>MnSn and Pd<sub>2</sub>MnSn, and (ii) the cubic XPt<sub>3</sub> compounds with X= V, Cr and Mn. The localization of the spin magnetic moment of the transition-metal atoms arises from the exclusion of the minority-spin electrons from these sites. We have also included in our study CoPt<sub>3</sub> which is a usual ferromagnet.

In all compounds under study due to the large spatial separation ( $\sim 4 \text{ \AA}$ ) of the magnetic transition metal atoms, the  $3d$  states belonging to different atoms overlap weakly and as a consequence the exchange coupling is indirect, mediated by the  $sp$  electrons. In the case of local ferromagnets a close look at the density of states (DOS) revealed that due to the  $sp-d$  mixing either the majority-spin DOS below the Fermi level or the minority-spin DOS just above the Fermi level are almost negligible, and therefore, the single-particle spin-flip Stoner excitations make a small contribution to the total excitation spectra at low energies, where collective spin-wave modes (magnons) dominate and the use of the frozen-magnon approximation in our calculations is justified. This reasoning is not applicable to CoPt<sub>3</sub> where no localization of the spin magnetic moment occurs. The calculated effective exchange parameters are long range and show RKKY-type oscillations. The Curie temperature is estimated within both the mean-field and the random-phase approximations and our calculations show that when the spin magnetic moment is concentrated at the transition-metal atom only the exchange constants between these atoms determine the value of the Curie temperature. In general,

the calculated Curie temperatures, exchange constants and spin-wave dispersion curves are in fair agreement with the available experimental data.

Overall we can conclude that the main criterion for the application of the frozen-magnon approximation is either the large value of the Stoner gap as in half-metallic ferromagnets (see discussion in Section 2) or a strong exchange splitting between the transition-metal majority- and minority-spin electronic bands as for the local moment ferromagnets under study in this article. Deviations of the estimated Curie temperature with respect to the experimental data occur when the ground-state electronic structure calculations overestimate the values of the spin magnetic moments as in VPt<sub>3</sub> or when the exchange splitting is not strong enough as in the usual ferromagnet CoPt<sub>3</sub>.

**Acknowledgements** Fruitful discussions with L.M. Sandratskii are acknowledged.

## References

1. Kübler J (2006) *J Phys: Condens Matter* 18:9795.
2. Thoene J, Chadov S, Fecher G, Felser C, Kübler J (2009) *J Phys D: Appl Phys* 42:084013.
3. Kurtulus Y, Dronskowski R, Samolyuk GD, Antropov VP (2005) *Phys Rev B* 71:014425.
4. Meinert M, Schmalhorst, Reiss G (2011) *J Phys: Condens Matter* 23:036001.
5. Meinert M, Schmalhorst, Reiss G (2011) *J Phys: Condens Matter* 23:116005.
6. Bose SK, Kudrnovsky J, Drchal V, Turek I (2010) *Phys Rev B* 82:174402.
7. Lezaic M, Mavropoulos Ph, Enkovaara J, Bihlmayer G, Blügel S (2006) *Phys Rev Lett* 97:026404.
8. Buchelnikov V D, Sokolovskiy V V, Herper H C, Ebert H, Gruner M E, Taskaev S V, Khovaylo V V, Hucht A, Dannenberg A, Ogura M, Akai H, Acet M, Entel P (2010) *Phys Rev B* 81:094411.
9. Ghosh S, Sanyal B (2010) *J Phys Condens Matter* 22:346001.
10. Bouzerar G, Kudrnovský J, Bergqvist L, Bruno P (2003) *Phys Rev B* 68:081203(R).
11. Sandratskii LM, Bruno P (2002) *Phys Rev B* 66:134435.
12. Liechtenstein A I, Katsnelson M I, Antropov V P and Gubanov V A (1987) *J Magn Magn Mater* 67:65.
13. Glazer J, Tossati E (1984) *Sol St Commun* 52:905.
14. Laref A, Şaşıoğlu E, Galanakis I (2011) *J Phys: Condens Matter* 23:296001.
15. Pajda M, Kudrnovsky J, Turek I, Drchal V, Bruno P (2001) *Phys Rev B* 64:174402.
16. Williams AR, Kübler J, Gelatt CD (1979) *Phys Rev B* 19:6094.
17. Andersen OK (1975) *Phys Rev B* 12:3060.
18. Perdew JP, Wang Y (1992) *Phys Rev B* 45:13244.
19. Şaşıoğlu E, Sandratskii LM, Bruno P (2004) *Phys Rev B* 70:024427.
20. Buczek P, Ernst A, Bruno P, Sandratskii LM (2009) *Phys Rev Lett* 102:247206.
21. Anderson PW (1963) Theory of magnetic exchange interactions: Exchange in insulators and semiconductors In: Seitz F, Turnbull F (eds) *Solid State Physics Vol 14*. Academic Press, New York, pp 99-214.
22. Şaşıoğlu E, Sandratskii LM, Bruno P, Galanakis I (2005) *Phys Rev B* 72:184415.
23. Şaşıoğlu E, Sandratskii LM, Bruno P (2005) *J Appl Phys* 98:063523.
24. Galanakis I, Özdoğan K, Şaşıoğlu E (2008) *J Appl Phys* 104:083916.
25. Sandratskii LM, Singer R, Şaşıoğlu E (2007) *Phys Rev B* 76:184406.
26. Galanakis I, Özdoğan K, Şaşıoğlu E, Aktaş B (2007) *Phys Rev B* 75:172405.
27. Galanakis I, Şaşıoğlu E (2011) *Appl Phys Lett* 99:052509.
28. Şaşıoğlu E, Galanakis I, Sandratskii LM, Bruno P (2005) *J Phys: Condens Matter* 17:3915.
29. Hortamani M, Sandratskii L, Kratzer P, Mertig I, Scheffler M (2008) *Phys Rev B* 78:104402.
30. Hortamani M, Sandratskii L, Kratzer P, Mertig I (2009) *New J Phys* 11:125009.
31. Gao GY, Yao KL, Şaşıoğlu E, Sandratskii LM, Liu ZL, Jiang JL (2007) *Phys Rev B* 75:174442.
32. Gao GY, Yao KL (2007) *Appl Phys Lett* 91:082512.
33. Şaşıoğlu E (2009) *Phys Rev B* 79:100406(R).
34. Sandratskii LM (2008) *Phys Rev B* 78:094425.
35. Şaşıoğlu E, Sandratskii LM, Bruno P (2006) *Appl Phys Lett* 89:222508.
36. Şaşıoğlu E, Sandratskii LM, Bruno P (2008) *Phys Rev B* 77:064417.
37. Kübler J, William AR, Sommers CB (1983) *Phys Rev B* 28:1745.
38. Shirai M, Maeshima H, Suzuki N (1995) *J Magn Magn Mater* 140-144:105.
39. Kulatov ET, Uspenskii YuA, Halilov SV (1996) *J Magn Magn Mater* 163:331.
40. Galanakis I, Alouani M, Dreyssé H (2002) *J Magn Magn Mater* 242-245:27.
41. Kwon Y, Rho TH, Lee S, Hong SC (2003) *J Appl Phys* 93:7151.
42. Iwashita K, Oguchi T, Jo T (1996) *Phys Rev B* 54:1159
43. Galanakis I, Alouani M, Dreyssé H (2000) *Phys Rev B* 62:6475.
44. Oppeneer PM, Galanakis I, Grechnev A, Eriksson O (2002) *J Magn Magn Mater* 240:371.
45. Galanakis I, Alouani M, Oppeneer PM, Dreyssé H, Eriksson O (2001) *J Phys: Condens Matter* 13:4553.
46. Pickart SJ, Nathans R (1963) *J Appl Phys* 34:1203.
47. Menzinger F, Paoletti A (1966) *Phys Rev* 143:365.
48. Bacon GE, Crangle J (1963) *Proc R Soc A* 272:387-405;
49. Kawakami M, Goto T (1979) *J Phys Soc Jpn* 46:1492.
50. Grange W, Maret M, Kappler J-P, Vogel J, Fontaine A, Petroff F, Krill G, Rogalev A, Goulon J, Finazzi M, Brookes NB (1998) *Phys Rev B* 58:6298.
51. Imada S, Muro T, Shishidou T, Suga S, Maruyama H, Kobayashi K, Yamazaki H, Kanomata T (1999) *Phys Rev B* 59:8752.
52. Lange RJ, Lee SJ, Lynch DW, Canfield PC, Harmon BN, Zollner S (1998) *Phys Rev B* 58:351.
53. Maret M, Bley F, Meneghini C, Albrecht M, Köhler J, Bucher E, Hazemann JL (2005) *J Phys: Condens Matter* 17:2529.
54. Tajima K, Ishikawa Y, Webster PJ, Stringfellow MW, Tocchetti D, Zebeck KRA (1977) *J Phys Soc Jpn* 43:483.
55. Noda Y, Ishikawa Y (1976) *J Phys Soc Jpn* 40:690.
56. Paul DMcK, Stirling WG (1979) *J Phys F: Metal Phys* 9:2439.
57. Bruno P (2003) *Phys Rev Lett* 90:087205.